Article

Significant winter Atlantic Niño effect on ENSO and its future projection

Check for updates

Jae-Heung Park [1] ✉, Young-Min Yang [2,3,4], Yoo-Geun Ham [5], Hyun-Su Jo [6], Hyo-Jin Park [7], So-Eun Park[7], Chao Liu [8], Gagan Mandal [8], Soon-Il An [7,8,9] & Jong-Seong Kug [1,10] ✉

The Atlantic Niño, a primary climatic variability mode in the equatorial Atlantic Ocean, exhibits pronounced variability not only in boreal summer but also in winter. However, the role of the winter Atlantic Niño in trans-basin interactions remains underexplored compared to its summer counterpart. Through analysis of observational reanalysis data since the mid-twentieth century, here we found that the winter Atlantic Niño significantly influences the development of El Niño–Southern Oscillation (ENSO), surpassing the impact of summer Atlantic Niño, with a longer lead time. This effect is reasonably captured in the CMIP6 Historical simulations from a multi-model ensemble perspective. Further analysis of the global warming scenario projects that the influence of winter Atlantic Niño on ENSO will persist into the future, in contrast to the reduced impact of summer Atlantic Niño. Therefore, these findings underscore the importance of further investigating the winter Atlantic Niño to gain a comprehensive understanding of trans-basin interactions and their future changes.

Manifested by various air-sea coupled processes[1–7], the Atlantic Niño is widely recognized as a leading mode of climatic variability in the tropical Atlantic Ocean on interannual time scales[8–12]. It exhibits its strongest variability in the boreal summer season (for convenience, seasons in this study follow those of the northern hemisphere) when the climatological mean thermocline depth along the equatorial Atlantic becomes shallower, accompanied by intensified mean easterly winds. In its positive phase, the sea surface temperature (SST) anomaly (SSTA) along the equatorial Atlantic becomes warm with westerly wind anomalies, and vice versa in its negative phase[3,8,10,12–15].

The Atlantic Niño events also involve precipitation changes around the Gulf of Guinea, the western coast of equatorial Africa[16–22], and Northeast Brazil[23], as well as the development of hurricanes[24]. On seasonal timescales, it is accompanied by a displacement of the Intertropical Convergence Zone (ITCZ) from the South America to the Atlantic Ocean[13,25]. This shift in the ITCZ induces modifications in deep convection, giving rise to stationary Rossby waves that propagate into the mid-latitudes. Consequently, Atlantic Niño events influence the North Atlantic Oscillation[26] and rainfall over the Mediterranean Sea and Europe[11,27]. Simultaneously, through modulations of the Walker circulation[28], the Atlantic Niño both affects and is affected by

other major climatic phenomena such as El Niño–Southern Oscillation (ENSO)[29–38] and the Indian Ocean Dipole[39], which are regarded as crucial drivers of climate variability in the Pacific and Indian Oceans, respectively. Given its substantial climatic and socioeconomic impacts[21,24,40], the Atlantic Niño has been of extensive interest.

While a typical Atlantic Niño is commonly characterized by an SSTA loading center in the eastern equatorial Atlantic during the summer, recent studies have revealed a variety of spatiotemporal evolution patterns for this phenomenon[41,42]. For example, unlike the consistent pattern previously assumed, the center of Atlantic Niño events is occasionally found in the central Atlantic region[42]. Furthermore, the onset and dissipation timings of these events display considerable diversity[41]. Particularly, Atlantic Niño events are frequently observed during the winter[43,44], coinciding with the second shallowest thermocline with easterly winds in that season[45]. To differentiate this winter occurrence from the more commonly studied summer Atlantic Niño (a.k.a., Atlantic Niño I[45]), in this study, it is termed the winter Atlantic Niño (a.k.a., Atlantic Niño II[45]).

Previous studies have examined the lead-lag relationship between the summer/winter Atlantic Niño and following ENSO with a half-year[29–38] and one-year lag[43,44], respectively. For the summer Atlantic Niño, its effect on

¹School of Earth and Environmental Sciences, Seoul National University, Seoul, South Korea. ² Department of Environment and Energy, Jeonbuk National University, Jeonju, South Korea. ³School of Civil, Environmental, Resources and Energy Engineering, Jeonbuk National University, Jeonju, South Korea. ⁴Soil Environment Research Center, Jeonbuk National University, Jeonju, South Korea. ⁵Department of Environmental Planning, Graduate School of Environmental Studies, Seoul National University, Seoul, South Korea. ⁶Environmental Planning Institute, Seoul National University, Seoul, South Korea. ⁷Department of Atmospheric Sciences, Yonsei University, Seoul, South Korea. ⁸Irreversible Climate Change Research Center, Yonsei University, Seoul, South Korea. ⁹Division of Environmental Science and Engineering, Pohang University of Science and Technology, Pohang, South Korea. ¹⁰Interdisciplinary Program in Artificial Intelligence, Seoul National University, Seoul, South Korea. ✉e-mail: jhp11010@gmail.com; jskug1@gmail.com
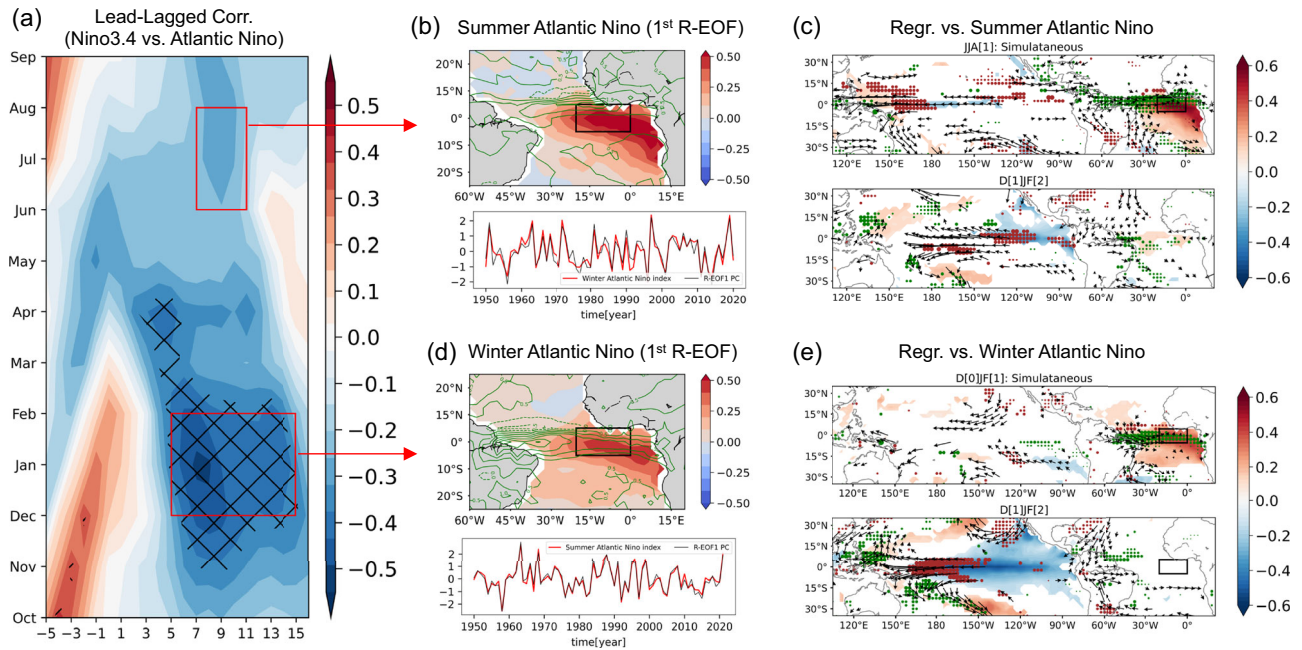
Fig. 1 | Atlantic Niño and its relationship with ENSO. a Lagged correlation between the monthly Atlantic Niño and ENSO indices for the period 1950–2021, where the x-axis indicates the number of months by which the Atlantic Niño index leads the Niño3.4 index (for positive values, the Atlantic Niño leads ENSO, and vice versa); the y-axis indicates the period from October to the following September. The negative maximum is found at 5–15 (x-axis) during December to February (y-axis), indicating that the Atlantic Niño in boreal winter negatively leads ENSO with a lag of 5–15 months. Hatching indicates the 99% confidence level using a two-tailed Student's t-test (degree of freedom: 50). b The first Rotating-EOF mode of SSTA in the tropical Atlantic Ocean during summer, along with its PC time series (black line in the bottom panel, normalized). The black box in the top panel indicates the area of Atlantic Niño (0–20°W, 5°S–5°N). The areal average of SSTA over the Atlantic Niño area in summer is illustrated by the red line in the bottom panel (normalized). Herein, green contours indicate anomalous summer precipitation regressed onto the summer Atlantic Nino index. The contour interval is 0.5 mm/day (solid for positive and dashed for negative; the zero line is omitted). c Anomalies of SST (shading, shading bar at right, 95%), low-level wind (850 hPa, vector, 95%), and precipitation (green and brown dots for positive and negative, 95%) in JJA[1] (top) and D[1]JF[2] (bottom) regressed onto the normalized summer Atlantic Niño index (previous winter ENSO signals are linearly removed). d Similar to (b), but for winter. e Anomalies of SST (shading, shading bar at right, 95%), low-level wind (850 hPa, vector, 95%), and precipitation (green and brown dots for positive and negative, 95%) in D[0]JF[1] (top) and D[1]JF[2] (bottom) regressed on to the normalized winter Atlantic Niño index (simultaneous winter ENSO signals are linearly removed).

ENSO was found to be weak during the mid-twentieth century, but strengthened from the late twentieth to the early twenty-first century[29,43,44]. We found that their lagged correlation coefficient is −0.23 since the mid-twentieth century (1950–2021), which is not significant at the 95% confidence level. Note that the change in their correlation coefficient is negligible when previous ENSO signals are excluded from the summer Atlantic Niño index (Supplementary Table 1).

In contrast to the summer Atlantic Niño, the winter Atlantic Niño effect on ENSO was strong during the mid-twentieth century but became weaker during the late twentieth to early twenty-first century[43]. During 1950–2021, their lagged correlation coefficient became −0.41, significant at the 99% confidence level (when simultaneous ENSO signals are removed, it is −0.40). This result contrasts sharply with the summer Atlantic Niño–ENSO relationship, which was found to be statistically insignificant over the same period. Notably, over the same period, the ENSO connection is most prominent with the winter Atlantic Niño, rather than with other primary climate variability modes, such as the Northern Tropical Atlantic (−0.32)[46–49] and the Atlantic Warm Pool[50,51] (a.k.a., Western Hemisphere Warm Pool[52,53], −0.22) (Supplementary Table 1). This implies that among the climate variability modes in the Atlantic Ocean, the one most relevant to the development of ENSO over the last seven decades could be the winter Atlantic Niño.

This simple correlation analysis implies the significant role of the winter Atlantic Niño in inter-basin interactions. Nevertheless, unfortunately the winter Atlantic Niño effect on ENSO has not been well investigated so far. Furthermore, there has been a lack of evaluation regarding the capability of current climate models to simulate the relationship between the winter Atlantic Niño and ENSO.

In this view, we examine the observed winter Atlantic Niño effect on ENSO in this study by analyzing the reanalysis dataset from 1950 to 2021. Additionally, we aim to assess the fidelity of climate models participating in the Coupled Model Intercomparison Project Phase 6 (CMIP6) in capturing the lagged relationship between the winter Atlantic Niño and subsequent ENSO events. Based on this assessment, we will also address its future projection. Through our analysis, we propose that the significant winter Atlantic Niño effect on ENSO will persist under global warming, in contrast to the weakened summer Atlantic Niño–ENSO connection.

Result

Observed relationship between the Atlantic Niño and ENSO (1950–2021)

We first obtained the monthly indices for the Atlantic Niño and ENSO by averaging the SSTA in the eastern equatorial Atlantic (0–20°W and 5°S–5°N) and the Niño3.4 region (120–170°W, 5°S–5°N), respectively. To examine their relationship, we conducted a lead-lagged correlation analysis spanning from 1950 to 2021 (864 months). In Fig. 1a, the negative (positive) values on the x-axis indicate how many months the ENSO (Atlantic Niño) leads the Atlantic Niño (ENSO), while the y-axis represents the calendar months of the leading index. For example, the bottom left area in Fig. 1a shows that ENSO in October to December positively precedes the Atlantic Niño with a lag of 2–4 months. This result indicates that the ENSO influence appears relatively modest, consistent with findings from prior studies.

When it comes to the Atlantic Niño-leading-ENSO signals, the upper red box in Fig. 1a indicates that the Atlantic Niño from June to August negatively leads ENSO, roughly with a lag of 9 months, and these signals are modest. Meanwhile, the Atlantic Niño from December to February

significantly leads ENSO with a lag ranging from 5 to 15 months, as shown in the bottom red box in Fig. 1a. These results indicate that ENSO has a close relationship with the previous winter Atlantic Niño, rather than with the previous summer Atlantic Niño.

Building upon the aforementioned results, we investigated the spatiotemporal variability of Atlantic Niño during both summer and winter, along with their subsequent effects on ENSO in the following winter. To comprehend the variability of the summer Atlantic Niño, we applied the Rotating-Empirical Orthogonal Function (R-EOF) analysis to the SSTA in the tropical Atlantic in summer[54] (Methods). As depicted in Fig. 1b, the 1st R-EOF mode, explaining 35.5% of the total variability, reveals a distinct spatial pattern characterized by strong SSTA amplitude extending from the eastern equatorial Atlantic Ocean to the subtropical western coast of South Africa. This spatial pattern resembles that of the summer Atlantic Niño. Its principal component (PC) time series is illustrated in Fig. 1b along with the summer Atlantic Niño index which is obtained by averaging the monthly Atlantic Niño index over the JJA season. Their correlation coefficient is higher than 0.9, indicating that the 1st R-EOF mode represents a physical mode[55]. Additionally, the green contour lines indicate anomalous precipitation regressed onto the summer Atlantic Niño index. Herein, the precipitation center is located over the northern area of the Atlantic Niño region (15°W, 5°N) toward the Sahel, in association with the northward-displaced ITCZ in summer.

Figure 1c illustrates anomalies of SST, low-level wind (850 hPa), and precipitation regressed onto the summer Atlantic Niño index. In JJA[1], SSTA warming is observed along the equatorial Atlantic, accompanied by westerly winds and enhanced precipitation, consistent with the features of the summer Atlantic Niño (Fig. 1b). The modulation of the Walker circulation by summer Atlantic Niño results in decreased precipitation over the equatorial Pacific Ocean, leading to low-level easterly winds and subsequent SSTA cooling in that region. Due to the Bjerknes feedback, the low-level easterly winds are still observed with SST cooling in the equatorial eastern Pacific in D[1]JF[2], despite the weak signals.

Subsequently, we applied the R-EOF method to the SSTA in the tropical Atlantic, this time focusing on winter. As illustrated in Fig. 1d, the 1st R-EOF mode accounts for 23.3% of the total variability and exhibits a spatial pattern akin to that of the summer Atlantic Niño, implying a similar underlying development mechanism. Its PC time series has a high correlation coefficient (>0.9) with the winter Atlantic Niño index, which is obtained by averaging the monthly Atlantic Niño index over the DJF season (Fig. 1d). This robust correlation underscores the physical relevance of the identified R-EOF mode in characterizing the winter Atlantic Niño phenomenon.

In Fig. 1d, the green contours depict anomalous precipitation in the DJF season regressed onto the winter Atlantic Niño index. Unlike the precipitation patterns associated with the summer Atlantic Niño, where the precipitation center shifts toward the Sahel region (Fig. 1b), the strongest precipitation anomalies linked to the winter Atlantic Niño are found from the mouth of the Amazon River to the western Atlantic Ocean along the equator. This is due to the southward movement of the Atlantic ITCZ toward South America, coinciding with the South American monsoon. Previous studies suggest that the Atlantic Ocean's influence on the Pacific Ocean tends to increase when anomalous precipitation in the tropical Atlantic shifts westward and closer to the equator[35,36]. This provides a clue as to why the winter Atlantic Niño effectively affects the Pacific climate.

To investigate how the winter Atlantic Niño affects the development of ENSO[43], anomalies of SST, low-level wind (850 hPa), and precipitation were regressed onto the winter Atlantic Niño index. In D[0]JF[1] (where, "1" indicates the decaying year of the winter Atlantic Niño) (Fig. 1e), SSTA warming is observed along the equatorial Atlantic with westerly wind anomalies and enhanced precipitation (please refer to Supplementary Fig. 1 for other seasons). Concurrently, low-level cyclonic circulation is located near Eastern Brazil (40°W) in both hemispheres, indicative of a Gill-type response to the equatorial atmospheric latent heat forcing. Since solar radiation faces the southern hemisphere in this season, precipitation along

the equatorial Atlantic is greater in the southern hemisphere than in the northern hemisphere. Over the Pacific, northeasterly wind anomalies are observed over the off-equatorial North Pacific. These easterly wind anomalies in boreal spring propagate toward the equator (Supplementary Fig. 1), facilitating the trade wind discharge[44,56,57]. Through the Bjerknes feedback, which is driven by the easterly wind along the equator in the following seasons, La Niña develops in the following winter (D[1]JF[2]). It is worth noting that these results remain consistent when other reanalysis datasets, such as ERSSTv5 and HadISST, are utilized (Supplementary Figs. 2, 3). We also note that the existence of previous Summer (JJA[0]) Atlantic Nino events does not affect these results (Supplementary Fig. 4), due to their low correlation coefficient (0.25; Supplementary Table 1).

Winter Atlantic Niño effect on ENSO in the historical and global warming scenario

Observational analysis during the last seven decades indicates that the winter Atlantic Niño exerts a more significant effect on ENSO, compared to the summer Atlantic Niño. Based on these results, we sought to investigate how current climate models participating in CMIP6 simulate the winter Atlantic Niño effect on ENSO in the Historical and SSP585 simulations (refer to Table 1 for climate models). To do this, we followed the same process as the observational analysis to obtain the winter Atlantic Niño and ENSO indices. Then, the 1-year lagged relationship between the winter Atlantic Niño (D[0]JF[1]) and ENSO (D[1]JF[2]) indices was examined.

Figure 2a indicates the lagged correlation coefficients between them for each climate model, as well as for their Multi-Model Ensemble (MME). For the Historical simulations, the correlation coefficients across climate models exhibit a wide range, varying from −0.47 for TaiESM1 to 0.17 for MPI-ESM1-2-LR, with 23 out of 30 climate models showing a negative correlation. As a result, the MME is −0.11, which is seemingly small but statistically significant at the 99% confidence level based on the Student's t-test with a large degree of freedom. For the SSP585 simulations, 25 out of 30 climate models show a negative correlation. Accordingly, compared to the Historical simulation, their MME is slightly increased to −0.15 (99% confidence level).

In addition to the correlation coefficient, regression coefficients in each climate model were also analyzed to infer the actual change in ENSO amplitude concerning variations in the winter Atlantic Niño. To this end, the original ENSO index (not normalized) is regressed onto the normalized winter Atlantic Niño index (y-axis in Fig. 2b). In the figure, the x-axis represents the correlation coefficients from Fig. 2a, wherein the R-squared value is greater than 0.9, indicating a pronounced linear relationship between the correlation and regression coefficients. The slope is 3.89, implying that a correlation coefficient of 0.1 in a particular climate model corresponds to a change in the ENSO index of approximately −0.4 °C per standard deviation of the Atlantic Niño.

Table 1 | List of climate models from CMIP6 utilized in the present study

CMIP6 Models		
ACCESS-CM2	E3SM-1-1-ECA	IPSL-CM6A-LR
ACCESS-ESM1-5	EC-Earth3	KACE-1-0-G
AWI-CM-1-1-MR	EC-Earth3-Veg	MIROC6
BCC-CSM2-MR	EC-Earth3-Veg-LR	MPI-ESM1-2-HR
CanESM5	FGOALS-f3-L	MPI-ESM1-2-LR
CESM2	FGOALS-g3	MRI-ESM2-0
CIESM	FIO-ESM-2-0	NESM3
CESM2-WACCM	GFDL-ESM4	NorESM2-LM
CMCC-CM2-SR5	INM-CM4-8	NorESM2-MM
E3SM-1-1	INM-CM5-0	TaiESM1

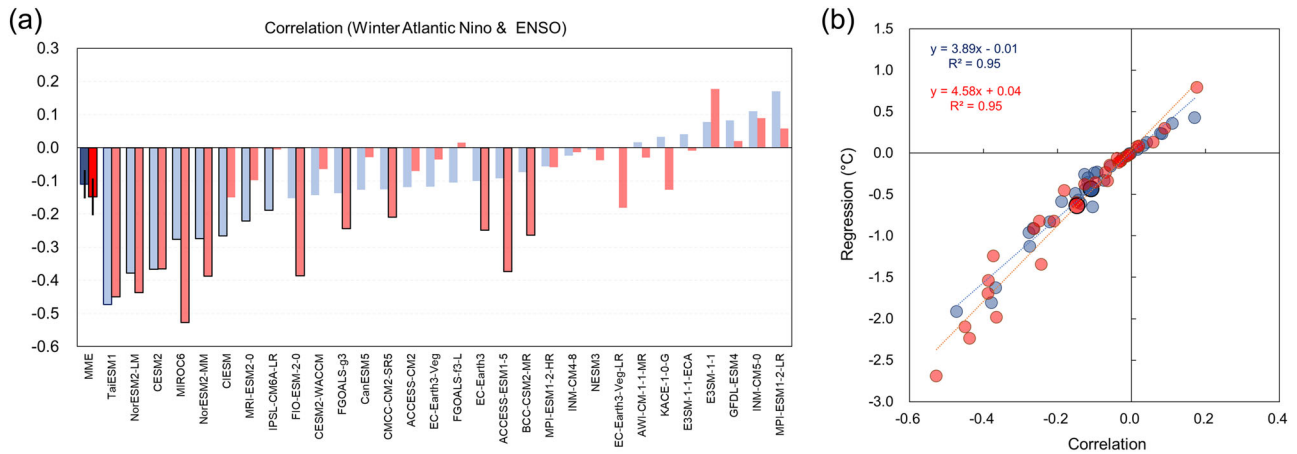Each climate model reserve SST, precipitation, and low-level wind (U, V) dataset.

Fig. 2 | The relationship between the Winter Atlantic Niño and ENSO in the Historical and SSP585 simulations from CMIP6. a The lagged correlation coefficients between the winter Atlantic Niño index (D[0]JF[1]) and the ENSO index (D[1]JF[2]) across 30 climate models from the Historical (pale blue, 1850–2014) and SSP585 (pale red, 2015–2100) simulations in CMIP6 are shown (Table 1). Their MMEs are illustrated on the leftmost side in blue and red. Black borders around each bar indicate statistical significance at the 95% confidence level based on the Student's *t*-test, with degrees of freedom fixed at 120 for Historical and 70 for SSP585 simulations. Error bars for the MMEs represent the 95% confidence interval derived from a bootstrap method (10,000 times). b A scatter plot of correlation (x-axis) and regression (y-axis, °C) between the winter Atlantic Niño (D[0]JF[1], normalized) and the ENSO (D[1]JF[2], unnormalized) index is presented. Pale blue and pale red dots represent climate model results from the Historical and SSP585 simulations, with their MMEs marked by blue and red dots. The regressed lines are shown as dotted pale blue and pale red lines.
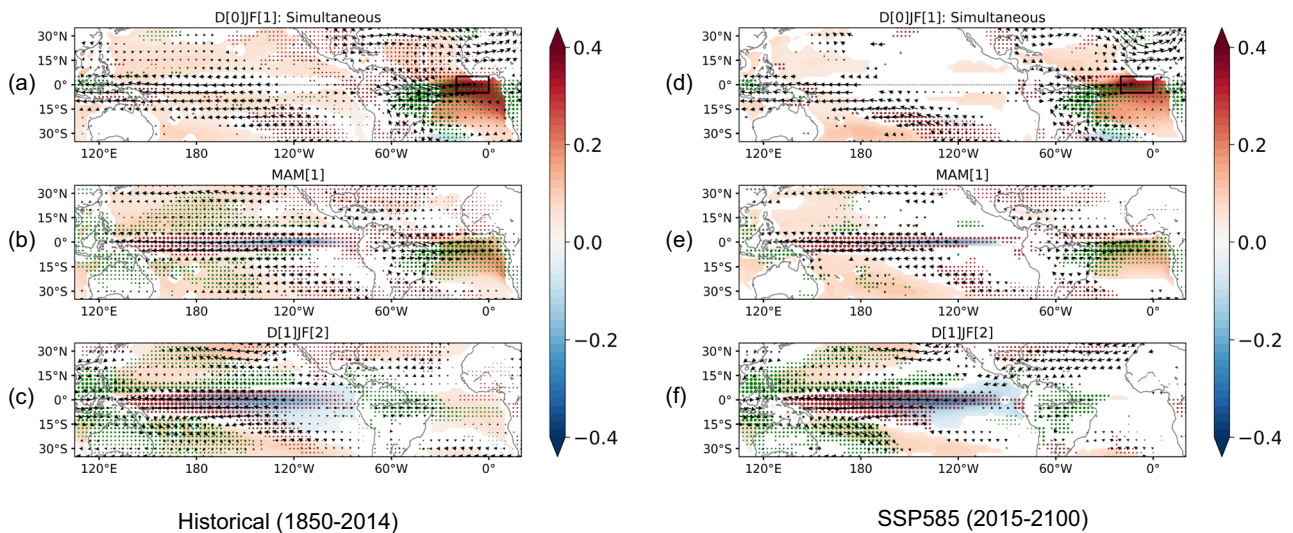
Regr. vs. Atlantic-Nino Index

Fig. 3 | Spatiotemporal evolution patterns of oceanic and atmospheric states regarding the winter Atlantic Niño in CMIP6. a MME of anomalies of SST (°C, shading bar at right), low-level wind (vector, at 850 hPa), and precipitation (dots, green and brown for positive and negative) in D[0]JF[1] regressed onto the winter Atlantic Niño index (D[0]JF[1]) in the Historical simulations (1850–2014). b, c Same as (a), but in MAM[1] and D[1]JF[2], respectively. The marked SST, wind, and precipitation reflect a 99% confidence level based on the Student's *t*-test. d–f Similar to (a–c), but with SSP585 simulations (2015–2100).

Similarly, the slope is about 4.58 for SSP585 simulation (Fig. 2b), which is stronger than that of the Historical simulations.

The above results suggest that the climate models in CMIP6 reasonably simulate the winter Atlantic Niño-leading-ENSO relationship from an MME perspective. To examine the processes by which the winter Atlantic Niño affects following ENSO events, SST, low-level wind, and precipitation anomalies are regressed onto the winter Atlantic Niño in each climate model, and the results are averaged. Figure 3a illustrates the simultaneous oceanic and atmospheric states when winter Atlantic Niño events occur in the Historical simulations. Over the Atlantic Ocean, SSTA warming occurs with westerly winds and enhanced precipitation, with stronger signals in the southern hemisphere than in the northern hemisphere, mirroring observations. However, the overall structure of the winter Atlantic Niño is meridionally and zonally wider than observed. Consequently, a pronounced modification of the Walker circulation is evident, characterized by strong low-level winds over the Pacific Ocean. From MAM to DJF, the signals over the Atlantic Ocean gradually decay, while those over the Pacific Ocean grow due to Bjerknes feedback. In the case of the SSP585 simulations, the overall evolutionary processes associated with the winter Atlantic Niño are consistent with those in the Historical simulations (Fig. 3d, e). In
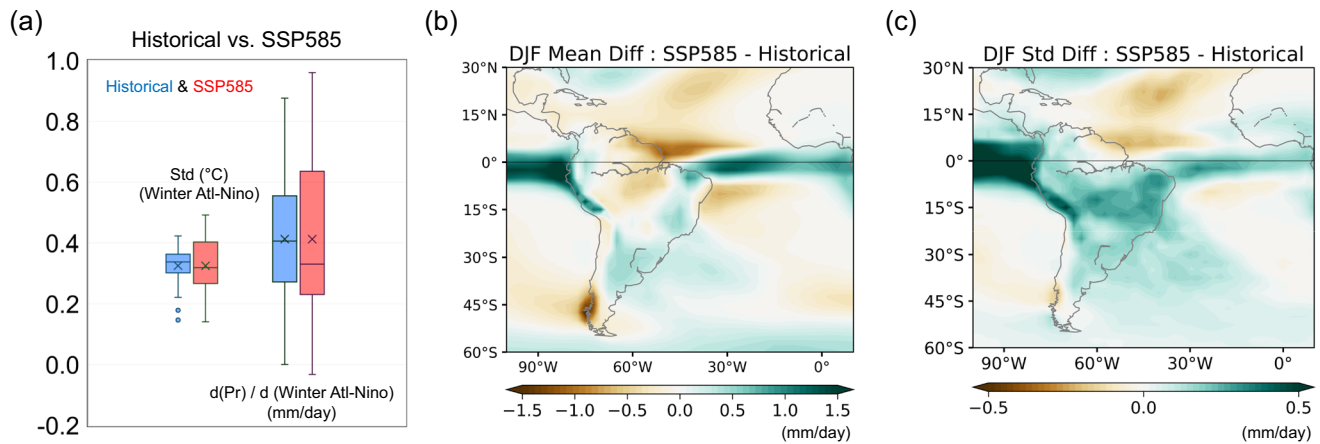
Fig. 4 | Variability of the winter Atlantic Niño and precipitation responses to it with respect to the mean state changes between Historical and SSP585 simulations. a The box-whisker plot shows the standard deviation of the winter Atlantic Niño (left, °C) and the precipitation response (0–45°W and 0–5°S, mm/day) to the winter Atlantic Niño (right) for Historical (blue) and SSP585 (red) simulations. In the box plot, the bottom, middle, and top edges represent the 25th percentile (First Quartile, Q1), the 50th percentile (Second Quartile, Q2, or median), and the 75th percentile (Third Quartile, Q3) of the data, respectively. The Interquartile Range (IQR) is calculated as Q3 minus Q1. The whiskers extend to the smallest and largest values within 1.5 times the IQR from Q1 and Q3, respectively. Data points outside the whiskers are considered outliers. The mean and outliers are marked by an "x" and dots, respectively. **b** Differences in climatological mean precipitation (shading) in the DJF season between SSP585 and Historical simulations. **c** Differences in standard deviation of precipitation (shading) in the DJF season between SSP585 and Historical simulations.

short, these findings suggest that the significant winter Atlantic Niño effect on ENSO is expected to persist during the global warming period.

Meanwhile, several climate models underestimate or even simulate an opposite correlation between the winter Atlantic Niño and ENSO (Fig. 2a). Hence, to appropriately infer future changes in the relationship between the winter Atlantic Niño and ENSO, it would be reasonable to analyze only those climate models that can faithfully capture the Atlantic Niño−ENSO correlation. In this regard, we selected 8 models that significantly simulate the Atlantic Niño−ENSO correlation in the Historical simulation as the "Best models" (Fig. 2a): TaiESM1, NorESM2-LM, CESM2, MIROC6, NorESM2-MM, CIESM, MRI-ESM2-0, and IPSL-CM6A-LR. For these Best models, their MME of the 1-year lag correlation between winter Atlantic Niño and ENSO for both the Historical and SSP585 simulations are −0.31 and −0.30, respectively. Furthermore, by examining the lead-lagged regression results using the Best models, we confirmed that the correlation between the winter Atlantic Niño and ENSO remains significant under future climate conditions (Supplementary Fig. 5).

Atmospheric responses to the winter Atlantic Niño in the Historical and SSP585 simulations

Previous studies have suggested that the summer Atlantic Niño effect on ENSO is likely to be weakened under greenhouse warming[58]. This weakening has been attributed to the reduced precipitation responses over the equatorial Atlantic Ocean and the decreased variability of the summer Atlantic Niño[59]. In contrast, we have shown that the winter Atlantic Niño effect on ENSO is stronger than the summer Atlantic Niño effect and is expected to be maintained under global warming. In light of these results, we aimed to examine changes in the variability of the winter Atlantic Niño under global warming. Additionally, to infer the change in the precipitation response, climatological mean state of precipitation over the equatorial Atlantic in winter and its variability were examined.

The left box-whisker plot in Fig. 4a illustrates the distribution of the standard deviation of the winter Atlantic Niño in climate models from Historical and SSP585 simulations. It is evident that the distribution in climate models from the SSP585 simulation is wider than that of the Historical simulation. However, the MMEs of Historical and

SSP585 simulations are both 0.326, indicating an insignificant difference between them. This suggests that the variability of the winter Atlantic Niño is expected to be maintained under global warming.

Meanwhile, the right box-whisker plot indicates the local precipitation response (0–45°W and 0–5°S) to the winter Atlantic Niño. Similar to the standard deviation of the winter Atlantic Niño, the distribution of precipitation response spreads widely in the SSP585 simulations, compared to the Historical simulations. However, their MMEs are close to each other (0.413 for Historical and 0.412 for SSP585). This suggests that the local precipitation response to the winter Atlantic Niño under global warming is not significantly altered.

Considering the sustained atmospheric response over the equatorial Atlantic, we examined the changes in the climatological winter precipitation mean state under global warming. Figure 4b shows the difference in winter precipitation between SSP585 and Historical simulations, revealing intensified precipitation over the equatorial Atlantic and the South Atlantic Convergence Zone (SACZ) in the SSP585 simulation. This intensified mean precipitation accompanies an amplification in the standard deviation of precipitation over the equatorial Atlantic and SACZ area. Aligned with the enhanced mean precipitation and its variability, the precipitation response to the SST over the region is expected to be maintained, under enhanced atmospheric stability[60]. In summary, the sustained variability of the winter Atlantic Niño and the precipitation responses under global warming collectively contribute to the persistence of the winter Atlantic Niño effect on ENSO.

Discussion

The Atlantic Niño, recognized as the predominant climate variability mode in the equatorial Atlantic, has received considerable attention due to its profound impact on the climate of both nearby and distant regions. Previous research has primarily focused on the summer season when its variability peaks. However, it is worth noting that significant variability also occurs during the winter season. Despite this, research on the winter Atlantic Niño remains relatively scarce. In this context, we investigated the influence of the winter Atlantic Niño on subsequent ENSO events with a 1-year lag over the past 70 years. By examining this relationship, we aimed to shed light on the importance of the winter Atlantic Niño in shaping interannual climate variability and its implications for broader climate dynamics.

We have demonstrated that the winter Atlantic Niño exerts a significant and greater effect on ENSO compared to the summer Atlantic Niño. Furthermore, our analysis of Historical and SSP585 simulation from CMIP6 indicates that climate models are capable of reasonably simulating the relationship between the winter Atlantic Niño and subsequent ENSO events from an MME perspective. Given that the variability of the winter Atlantic Niño and the precipitation responses to it are projected to be maintained under global warming, in association with intensified mean precipitation over the equatorial Atlantic Ocean, we anticipate that its influence on ENSO will persist in the future. Therefore, we believe that further investigation of the winter Atlantic Niño will lead to a better understanding of trans-basin interactions and their implications for future climate dynamics. Note that this contrasts with the weakening influence of the summer Atlantic Niño on ENSO under global warming, which is attributed to the reduction in climatological summer mean precipitation and its decreased variability in the equatorial Atlantic (Supplementary Fig. 6).

As discussed above, the MME of climate models appears to reasonably capture the effect of the winter Atlantic Niño on ENSO. However, it is important to acknowledge that most climate models struggle to accurately reproduce the spatiotemporal characteristics of the Atlantic Nino associated with the climatological mean state. For example, observations reveal that the Atlantic Niño exhibits peak phases during both summer and winter, yet climate models rarely simulate these double peaks, thus failing to replicate such phenomena from an MME perspective (Supplementary Fig. 7).

Regarding the unrealistic simulation of the winter Atlantic Nino in climate models, the winter Atlantic Nino seems to be a decaying phase of the summer Atlantic Nino. To this end, we obtained the MME of anomalous SST regressed onto the winter Atlantic index from the previous summer (JJA[0]) to winter (D[0]JF[1]) in Historical simulation (Supplementary Fig. 8). The results show that a weak SSTA warming in the equatorial Atlantic region during summer intensifies through the fall and becomes stronger in winter. Consequently, the winter Atlantic Niño could be considered an independent mode from the summer Atlantic Niño even in climate models.

Furthermore, whereas the spatial variability of the winter Atlantic Niño in observations is well explained by R-EOF, climate models often fall short in adequately simulating this variability (Supplementary Fig. 9). These discrepancies may be attributed, in part, to the fact that observed re-intensification of the climatological low-level easterly wind and deepening of the thermocline along the equatorial Atlantic in boreal winter are not well reproduced in climate models. These issues regarding the simulation of the observed climatological mean state in climate models are well-documented in previous research[9,61]. Therefore, conducting an in-depth investigation to improve the climatological mean state in climate models would be beneficial for better simulating the Atlantic Niño and its influence.

Methods
Index
For both observation and CMIP6 analysis, the monthly Atlantic Niño index is defined as the areal averaged SSTA over the equatorial Atlantic Ocean (0–20°W, 5°S–5°N) in 1950–2021. To obtain the winter Atlantic Niño index, the average for December to February is calculated from the monthly Atlantic Niño index. When conducting correlation or regression analyses, the simultaneous winter (DJF) ENSO signal is removed linearly using regression analysis to exclude ENSO auto-correlation effects. For the summer Atlantic Niño index, June to August is averaged from the monthly Atlantic Niño index. When conducting correlation or regression analyses, the previous winter (DJF) ENSO signal is removed linearly using regression analysis to exclude ENSO auto-correlation effects. The ENSO index is retained by averaging SSTA over the Niño3.4 area (120°W–170°W and 5°S–5°N), with a focus on the DJF season.

Rotating EOF (R-EOF) analysis
EOF analysis is commonly used to extract the dominant physical climate modes that explain the total variability of a specific region well. However, since it relies solely on a mathematical approach, it is not always grounded in physical principles. Therefore, to complement the limitations of EOF and improve the physical interpretation, Rotating-EOF analysis is often employed by rotating the projected EOFs. In this study, varimax orthogonal rotation, which maximizes the total variance of the squared-loading coefficients was applied to the original EOFs[62,63].

Data availability
Reanalysis Dataset: We utilized the ECMWF Reanalysis v5 (ERA5[64]), which combines vast amounts of historical observations into global estimates using advanced modeling and data assimilation systems. Additionally, to confirm the robustness of the results, we also use the monthly dataset from the US NOAA National Center for Environmental Prediction Reanalysis 1 (NCEP-R1[65]), which is an assimilated dataset that employs a state-of-the-art analysis and forecast system. For SSTs, NOAA's Extended Reconstruction Sea Surface Temperature version 5 (ERSSTv5[66]) and Hadley Centre Sea Ice and Sea Surface Temperature data set (HadISST[67]) were selected, both of which are global monthly SST datasets. The analysis period for this study was from 1950 to 2021. CMIP6 Dataset: For Historical and SSP585 simulations, we can reserve 30 climate models that provide SST, SLP, wind, and precipitation (Table 1). All of observational and CMIP6 data can be downloaded from open URL. ERA5: https://www.metoffice.gov.uk/hadobs/hadisst/data/download.html. NCEP-R1: https://psl.noaa.gov/data/gridded/data.ncep.reanalysis.html. ERSSTv5: https://www.esrl.noaa.gov/psd/data/data.php. HadISST: https://www.metoffice.gov.uk/hadobs/hadisst/data/download.html. CMIP6: https://aims2.llnl.gov/search/cmip6/.

Code availability
Codes used in the manuscript are available upon reasonable requests from J.-H. Park (jhp11010@gmail.com).

References
1. Zebiak, S. E. Air-sea interaction in the equatorial Atlantic region. *J. Clim.* **6**, 1567–1586 (1993).
2. Chang, P., Fang, Y., Saravanan, R., Ji, L. & Seidel, H. The cause of the fragile relationship between the Pacific El Nĩo and the Atlantic Nĩo. *Nature* **443**, 324–328 (2006).
3. Lübbecke, J. F. et al. Equatorial Atlantic variability—modes, mechanisms, and global teleconnections. *WIREs Clim. Chang.* **9**, e527 (2018).
4. Lübbecke, J. F. Climate science: tropical Atlantic warm events. *Nat. Geosci.* **6**, 22–23 (2013).
5. Foltz, G. R. & McPhaden, M. J. Abrupt equatorial wave-induced cooling of the Atlantic cold tongue in 2009. *Geophys. Res. Lett.* **37**, L24605 (2010).
6. Lübbecke, J. F., Böning, C. W., Keenlyside, N. S. & Xie, S.-P. On the connection between Benguela and equatorial Atlantic Niños and the role of the South Atlantic Anticyclone. *J. Geophys. Res. Ocean.* **115**, C09015 (2010).
7. Richter, I. et al. Multiple causes of interannual sea surface temperature variability in the equatorial Atlantic Ocean. *Nat. Geosci.* **6**, 43–47 (2013).
8. Keenlyside, N. S. & Latif, M. Understanding equatorial Atlantic interannual variability. *J. Clim.* **20**, 131–142 (2007).
9. Richter, I., Xie, S. P., Behera, S. K., Doi, T. & Masumoto, Y. Equatorial Atlantic variability and its relation to mean state biases in CMIP5. *Clim. Dyn.* **42**, 171–188 (2014).
10. Carton, J. A. & Huang, B. Warm events in the tropical Atlantic. *J. Phys. Oceanogr.* **24**, 888–903 (1994).
11. García-Serrano, J., Losada, T., Rodríguez-Fonseca, B. & Polo, I. Tropical Atlantic variability modes (1979–2002). part II: time-evolving atmospheric circulation related to SST-forced tropical convection. *J. Clim.* **21**, 6476–6497 (2008).

12. Polo, I., Rodríguez-Fonseca, B., Losada, T. & García-Serrano, J. Tropical Atlantic variability modes (1979-2002). Part I: time-evolving SST modes related to West African rainfall. *J. Clim.* **21**, 6457–6475 (2008).

13. Xie, S.-P. & Carton, J. A. Tropical Atlantic variability: patterns, mechanisms, and impacts. In Earth's Climate (eds Wang, C., Xie, S. P. & Carton, J. A.) 121–142 https://doi.org/10.1029/147GM07 (2004).

14. Lee, S. K. et al. On the Genesis of the 2021 Atlantic Niño. *Geophys. Res. Lett.* **50**, 1–10 (2023).

15. Lübbecke, J. F. & McPhaden, M. J. Symmetry of the Atlantic Niño mode. *Geophys. Res. Lett.* **44**, 965–973 (2017).

16. Brandt, P. et al. Equatorial upper-ocean dynamics and their interaction with the West African monsoon. *Atmos. Sci. Lett.* **12**, 24–30 (2011).

17. Rodríguez-Fonseca, B. et al. Interannual and decadal SST-forced responses of the West African monsoon. *Atmos. Sci. Lett.* **12**, 67–74 (2011).

18. Kucharski, F. et al. Atlantic forcing of Pacific decadal variability. *Clim. Dyn.* **46**, 2337–2351 (2016).

19. Giannini, A., Saravanan, R. & Chang, P. Oceanic forcing of Sahel rainfall on interannual to interdecadal time scales. *Science* **302**, 1027 LP–1030 (2003).

20. Losada, T. et al. A multi-model approach to the Atlantic Equatorial mode: impact on the West African monsoon. *Clim. Dyn.* **35**, 29–43 (2010).

21. Okumura, Y. & Xie, S.-P. Interaction of the Atlantic Equatorial Cold Tongue and the African Monsoon. *J. Clim.* **17**, 3589–3602 (2004).

22. Rodríguez-Fonseca, B. et al. Variability and predictability of West African droughts: a review on the role of sea surface temperature anomalies. *J. Clim.* **28**, 4034–4060 (2015).

23. Folland, C. K., Colman, A. W., Rowell, D. P. & Davey, M. K. Predictability of Northeast Brazil rainfall and real-time forecast skill, 1987–98. *J. Clim.* **14**, 1937–1958 (2001).

24. Kim, D. et al. Increase in Cape Verde hurricanes during Atlantic Niño. *Nat. Commun.* **14**, 3704 (2023).

25. Richter, I. et al. Phase locking of equatorial Atlantic variability through the seasonal migration of the ITCZ. *Clim. Dyn.* **48**, 3615–3629 (2017).

26. Peng, S., Robinson, W. A., Li, S. & Hoerling, M. P. Tropical Atlantic SST forcing of coupled North Atlantic seasonal responses. *J. Clim.* **18**, 480–496 (2005).

27. Kucharski, F., Bracco, A., Yoo, J. H. & Molteni, F. Atlantic forced component of the Indian monsoon interannual variability. *Geophys. Res. Lett.* **35**, L04706 (2008).

28. Wang, C. An overlooked feature of tropical climate: inter-Pacific-Atlantic variability. *Geophys. Res. Lett.* **33**, 1–5 (2006).

29. Rodríguez-Fonseca, B. et al. Are Atlantic Niños enhancing Pacific ENSO events in recent decades? *Geophys. Res. Lett.* **36**, L20705 (2009).

30. Ding, H., Keenlyside, N. S. & Latif, M. Impact of the Equatorial Atlantic on the El Niño Southern Oscillation. *Clim. Dyn.* **38**, 1965–1972 (2012).

31. Kucharski, F., Kang, I. S., Farneti, R. & Feudale, L. Tropical Pacific response to 20th century Atlantic warming. *Geophys. Res. Lett.* **38**, 1–5 (2011).

32. Kucharski, F., Syed, F. S., Burhan, A., Farah, I. & Gohar, A. Tropical Atlantic influence on Pacific variability and mean state in the twentieth century in observations and CMIP5. *Clim. Dyn.* **44**, 881–896 (2015).

33. Polo, I., Martin-Rey, M., Rodriguez-Fonseca, B., Kucharski, F. & Mechoso, C. R. Processes in the Pacific La Niña onset triggered by the Atlantic Niño. *Clim. Dyn.* **44**, 115–131 (2015).

34. Losada, T., Rodríguez-Fonseca, B., Roberto Mechoso, C., Mohino, E. & Castaño-Tierno, A. Changes in interannual tropical Atlantic–Pacific basin interactions modulated by a South Atlantic cooling. *J. Clim.* **35**, 4403–4416 (2022).

35. Martín-Rey, M., Polo, I., Rodríguez-Fonseca, B., Losada, T. & Lazar, A. Is there evidence of changes in tropical Atlantic variability modes under AMO phases in the observational record? *J. Clim.* **31**, 515–536 (2018).

36. Martín-Rey, M., Rodríguez-Fonseca, B., Polo, I. & Kucharski, F. On the Atlantic–Pacific Niños connection: a multidecadal modulated mode. *Clim. Dyn.* **43**, 3163–3178 (2014).

37. Lübbecke, J. F. & McPhaden, M. J. On the inconsistent relationship between Pacific and Atlantic Niños. *J. Clim.* **25**, 4294–4303 (2012).

38. Johnson, Z. F., Chikamoto, Y., Wang, S. Y. S., McPhaden, M. J. & Mochizuki, T. Pacific decadal oscillation remotely forced by the equatorial Pacific and the Atlantic Oceans. *Clim. Dyn.* **55**, 789–811 (2020).

39. Zhang, L. & Han, W. Indian Ocean dipole leads to Atlantic Niño. *Nat. Commun.* **12**, 5952 (2021).

40. Kucharski, F. et al. A gill–matsuno-type mechanism explains the tropical Atlantic influence on African and Indian monsoon rainfall. *Q. J. R. Meteorol. Soc.* **135**, 569–579 (2009).

41. Vallès-Casanova, I., Lee, S.-K., Foltz, G. R. & Pelegrí, J. L. On the spatiotemporal diversity of Atlantic Niño and associated rainfall variability over West Africa and South America. *Geophys. Res. Lett.* **47**, e2020GL087108 (2020).

42. Zhang, L. et al. Emergence of the Central Atlantic Niño. *Sci. Adv.* **9**, eadi5507 (2024).

43. Hounsou-Gbo, A. et al. Summer and winter Atlantic Niño: connections with ENSO and implications. *Clim. Dyn.* **55**, 2939–2956 (2020).

44. Park, J., Kug, J., Yang, Y., Park, H. & An, S. Distinct decadal modulation of Atlantic-Niño influence on ENSO. *Npj. Clim. Atmos. Sci.* **6**, 1–11 https://doi.org/10.1038/s41612-023-00429-9 (2023).

45. Okumura, Y. & Xie, S.-P. Some overlooked features of tropical Atlantic climate leading to a new niño-like phenomenon. *J. Clim.* **19**, 5859–5874 (2006).

46. Ham, Y. G., Kug, J. S., Park, J. Y. & Jin, F. F. Sea surface temperature in the north tropical Atlantic as a trigger for El Niño/Southern Oscillation events. *Nat. Geosci.* **6**, 112–116 (2013).

47. Wang, L., Yu, J. Y. & Paek, H. Enhanced biennial variability in the Pacific due to Atlantic capacitor effect. *Nat. Commun.* **8**, 14887 (2017).

48. Park, J. H. et al. Two regimes of inter-basin interactions between the Atlantic and Pacific Oceans on interannual timescales. *Npj Clim. Atmos. Sci.* **6**, 1–8 (2023).

49. Park, J.-H. et al. Role of the climatological North Pacific high in the North Tropical Atlantic–ENSO connection. *J. Clim.* **35**, 3215–3226 (2022).

50. Park, J. H., Kug, J. S., Li, T. & Behera, S. K. Predicting El niño beyond 1-year lead: effect of the western hemisphere warm pool. *Sci. Rep.* **8**, 1–8 (2018).

51. Park, J. H., Kug, J. S., An, S., & Li, T. Role of the western hemisphere warm pool in climate variability over the western North Pacific. *Clim. Dyn.* **53**, 2743–2755 (2019).

52. Wang, C., Enfield, D. B., Lee, S. K. & Landsea, C. W. Influences of the Atlantic warm pool on western hemisphere summer rainfall and Atlantic hurricanes. *J. Clim.* **19**, 3011–3028 (2006).

53. Enfield, D. B., Lee, S. K. & Wang, C. How are large western hemisphere warm pools formed? *Prog. Oceanogr.* **70**, 346–365 (2006).

54. Richman, M. B. Rotation of principal components. *J. Climatol.* **6**, 293–335 (1986).

55. Lian, T. & Chen, D. An evaluation of rotated of analysis and its application to tropical pacific SST variability. *J. Clim.* **25**, 5361–5373 (2012).

56. Anderson, B. T. On the joint role of subtropical atmospheric variability and equatorial subsurface heat content anomalies in initiating the onset of ENSO events. *J. Clim.* **20**, 1593–1599 (2007).

57. Di Lorenzo, E. et al. ENSO and meridional modes: a null hypothesis for Pacific climate variability. *Geophys. Res. Lett.* **42**, 9440–9448 (2015).

58. Jia, F. et al. Weakening Atlantic Niño–Pacific connection under greenhouse warming. *Sci. Adv.* **5**, eaax4111 (2019).

59. Crespo, L. R. et al. Weakening of the Atlantic Niño variability under global warming. *Nat. Clim. Chang.* **12**, 822–827 (2022).
60. Chou, C., Wu, T.-C. & Tan, P.-H. Changes in gross moist stability in the tropics under global warming. *Clim. Dyn.* **41**, 2481–2496 (2013).
61. Wang, C., Zhang, L., Lee, S. K., Wu, L. & Mechoso, C. R. A global perspective on CMIP5 climate model biases. *Nat. Clim. Chang.* **4**, 201–205 (2014).
62. Kaiser, H. F. The varimax criterion for analytic rotation in factor analysis. *Psychometrika* **23**, 187–200 (1958).
63. Hannachi, A. Tropospheric planetary wave dynamics and mixture modeling: two preferred regimes and a regime shift. *J. Atmos. Sci.* **64**, 3521–3541 (2007).
64. Hersbach, H. et al. The ERA5 global reanalysis. *Q. J. R. Meteorol. Soc.* **146**, 1999–2049 (2020).
65. Kistler, R. et al. The NCEP-NCAR 50-year reanalysis: monthly means CD-ROM and documentation. *Bull. Am. Meteorol. Soc.* **82**, 247–267 (2001).
66. Huang, B. et al. Extended reconstructed sea surface temperature, version 5 (ERSSTv5): upgrades, validations, and intercomparisons. *J. Clim.* **30**, 8179–8205 (2017).
67. Rayner, N. A. et al. Global analyses of sea surface temperature, sea ice, and night marine air temperature since the late nineteenth century. *J. Geophys. Res. Atmos*. **108**, 4407 (2003).

Acknowledgements

Author contributions

J.-H.P. initiated the research with the initial idea and produced the preliminary results. J.-S.K., Y.-M.Y., Y.-G.H., H.-S.J., H.-J.P., C.L., G.M., S.-E.P and S.-I.A. advanced the research through in-depth discussions. J.-H.P. conducted the analyses and prepared the figures with H.-J.P. and S.-E.P. All authors discussed the research results and reviewed the manuscript, which was first prepared by J.-H.P.

Competing interests

The authors declare no competing interests.

Additional information

Supplementary information The online version contains supplementary material available at https://doi.org/10.1038/s41612-024-00790-3.

Correspondence and requests for materials should be addressed to Jae-Heung Park or Jong-Seong Kug.

Reprints and permissions information is available at http://www.nature.com/reprints

Publisher's note Springer Nature remains neutral with regard to jurisdictional claims in published maps and institutional affiliations.